Cryo-EM structure of human Wntless in complex with Wnt3a

Qing Zhong
Westlake University
Fangfei Ye
Westlake University
Zaiyu Xiao
Westlake University
Yuanyuan Zhang
Westlake University
Gaoxingyu Huang
Westlake University
Xiechao Zhan
Westlake University
Ke Sun
Westlake University
Zhizhi Wang
ShanghaiTech University
Shanshan Cheng
ShanghaiTech University
Shan Feng
University of Notre Dame
Meng Xu
Westlake University
Xiuxiu Zhao
Westlake University
Jizhong Zhang
Westlake University
Peilong Lu
Westlake University https://orcid.org/0000-0001-5894-9268
Wenqing Xu
ShanghaiTech University
Qiang Zhou
Westlake University
Dan Ma (madan@westlake.edu.cn)

Westlake University https://orcid.org/0000-0002-6208-2262

Article

Keywords: Wnt signaling, Wnt secretion, WLS, Wnt3a, cryo-EM structure, Porcupine, palmitoleoylation, membrane protein, GPCR.

Posted Date: January 16th, 2021

DOI: https://doi.org/10.21203/rs.3.rs-144481/v1

Version of Record: A version of this preprint was published at Nature Communications on July 27th, 2021. See the published version at https://doi.org/10.1038/s41467-021-24731-3.

Cryo-EM structure of human Wntless in complex with Wnt3a

Qing Zhong[1,2,3,4#], Fangfei Ye[2,3,4#], Zaiyu Xiao[1,2,3,4#], Yuanyuan Zhang[2], Gaoxingyu Huang[2], Xiechao Zhan[2], Ke Sun[2], Zhizhi Wang[5], Shanshan Cheng[5], Shan Feng[2,6], Meng Xu[2], Xiuxiu Zhao[2,6], Jizhong Zhang[2], Peilong Lu[2,3,4], Wenqing Xu[5], **Qiang Zhou[2,3,4*], Dan Ma[2,3,4*]**

1. Fudan University, Shanghai, China
2. Key Laboratory of Structural Biology of Zhejiang Province, School of Life Sciences, Westlake University, Hangzhou, Zhejiang, China.
3. Westlake Laboratory of Life Sciences and Biomedicine, Hangzhou, Zhejiang, China.
4. Institute of Biology, Westlake Institute for Advanced Study, Hangzhou, Zhejiang, China.
5. School of Life Science and Technology, ShanghaiTech University, Shanghai, China
6. Mass Spectrometry Core Facility, The Biomedical Research Core Facility, Center for Research Equipment and Facilities, Westlake University, Hangzhou, Zhejiang

# These authors contributed equally: Qing Zhong, Fangfei Ye, Zaiyu Xiao.

* Corresponding email: madan@westlake.edu.cn, zhouqiang@westlake.edu.cn

Key Words: Wnt signaling; Wnt secretion; WLS; Wnt3a; cryo-EM structure; Porcupine; palmitoleoylation; membrane protein; GPCR.

Abstract

Wntless (WLS), an evolutionarily conserved multi-pass transmembrane protein, is essential for secretion of Wnt proteins. Wnt-triggered signaling pathways control many crucial life events, whereas aberrant Wnt signaling is tightly associated with many human diseases including cancers. Here, we report the cryo-EM structure of human WLS in complex with Wnt3a, the most widely studied Wnt, at 3.8 Å resolution. The transmembrane domain of WLS bears a GPCR fold, with a conserved core cavity and lateral opening. A β-hairpin of Wnt3a containing a conserved palmitoleoylation site has extensive interactions with the WLS luminal domain, and the tip region is accommodated in the WLS cavity. The flexibility of Wnt3a loop/hairpin regions involved in the multiple binding sites indicates a possible sequential release mechanism when Wnts are transferred to their receptors. We found Wnt3a palmitoleoylation site mutant has similar binding capability with WLS compared with wild type Wnt3a, suggesting palmitoleoylation is not essential for Wnt-WLS association. Our findings provide important insights into the molecular mechanism of Wnt palmitoleoylation, secretion and signaling.

Introduction

Wnt signaling is highly conserved among metazoans[1,2], and controls many critical events during early embryonic development, later growth, maintenance of adult tissue homeostasis, as well as self-renewal of stem cells[3,4]. Working together with other signaling pathways, Wnt signaling drives cell proliferation and differentiation in an appropriate manner, which is crucial for all the multicellular organisms. Mutations in Wnt signaling pathway genes that cause aberrant signaling activities are tightly associated with many human diseases including some aggressive metastatic cancers[5,6].

Wnt proteins comprise a family of secreted proteins[7,8]. They bind to highly conserved cell surface receptors[9-12] and trigger signaling cascades in target cells in either paracrine or autocrine manner[13]. Wnt proteins harbor a palmitoleate (PAM) modification in most circumstances, which is catalyzed by the *O*-acyltransferase Porcupine during Wnt maturation

in ER[14-17]. The subsequent secretion of Wnt proteins towards extracellular space relies on an evolutionarily conserved multi-pass transmembrane protein Wntless (WLS) [18-20].

WLS has been found to directly interact with Wnts throughout the secretory route initiated from ER, then Golgi, secretory vesicles and finally cell membrane [18,19,21,22]. After release of Wnts, WLS is recycled from cell membrane to ER by a retromer complex[23-25]. WLS is essential for Wnt secretion and downstream signaling, however, due to lack of structural information, the molecular mechanism of Wnt secretion remains poorly understood. It has also been shown that WLS is upregulated in some cancers and promote caner development, indicating WLS is a potential drug target for the treatment of Wnt-driven cancers [26-28]. Three-dimensional (3D) structure of WLS is in urgent need for understanding the mechanism for Wnt-secretion, as well as the discovery of new cancer therapeutics targeting Wnt signaling.

Here, we report a cryo-EM structure of wild type (WT) human WLS in complex with Wnt3a at 3.8 Å resolution. Wnt3a bound to WLS exhibits structural differences compared to the structure of its close homolog Wnt3 in the Wnt-Frizzled (cysteine-rich domain) complex. Our structure provides structural basis for understanding the molecular mechanism of WLS mediated Wnt secretion, and development of drugs for treatment of Wnt-driven cancers.

Results

Overall structure of the human WLS-Wnt3a complex

We co-expressed full-length human WLS and Wnt3a in HEK293S GnTI$^-$ cells co-infected with viruses generated from pEG BacMam vector [29]. In order to trap WLS-Wnt3a complex within cells, we treated the transfected cells with V-ATPase inhibitor bafilomycin A1 to suppress Wnt secretion [22,30]. We purified the WLS-Wnt3a complex by affinity chromatography followed by size exclusion chromatography (SEC). The homogeneity of protein samples was checked through negative staining for initial screening before cryo-EM sample preparation and data acquisition.

After data processing, we obtained a 3.8 Å resolution cryo-EM map (Fig. 1a and Supplementary Fig. 1, 2). We used a human Wnt3 structure model (hWnt3, PDB code: 6AHY) and a de novo predicted model of WLS (generated from trRosetta[31] and tFold [32]) to guide the

model building. The built model comprises 474 residues of 541-residue WLS and 308 residues of 334-residue Wnt3a (after cleavage of signal peptide), with the exception of parts of loop regions (Fig. 1b and Supplementary Table 1).

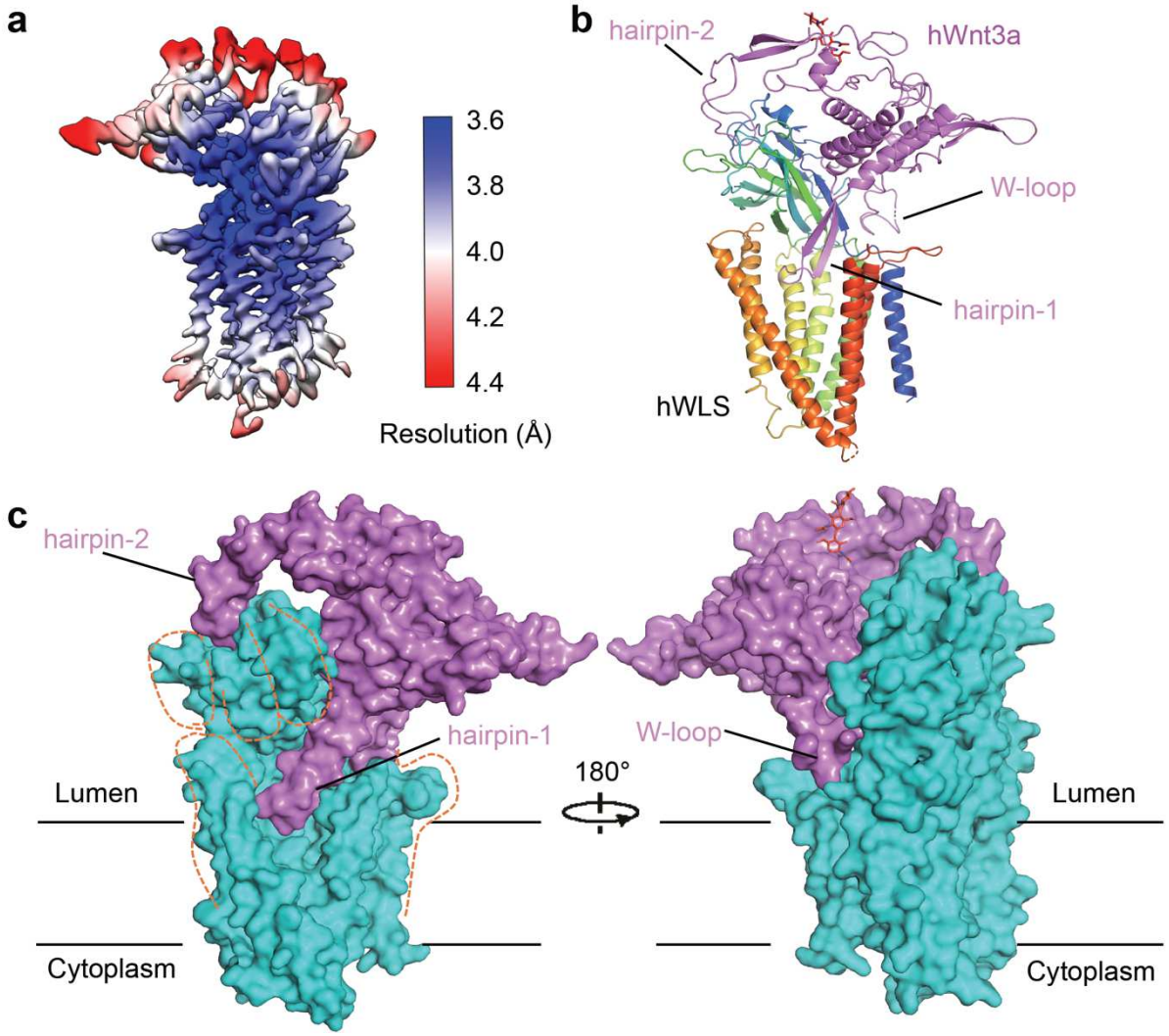

Fig. 1 Cryo-EM structure of human WLS in complex with Wnt3a. a Local resolution map of WLS-Wnt3a complex estimated with RELION. **b** Overall structure of the WLS-Wnt3a complex. WLS is shown in cartoon and colored in rainbow, with N-termini in blue and C-termini in red. Wnt3a is colored in magenta. The sugar moiety on Wnt3a is shown as sticks. **c** Complex structure is shown in surface with Wnt3a colored in magenta and WLS colored in cyan. The contour of hand shape of WLS is shown in orange dash lines. All structural figures are generated with PyMOL[33].

In the overall structure, Wnt3a perches on the luminal side of WLS with several β-hairpin and loop regions of Wnt3a (hairpin-1, hairpin-2 and W-loop) forming extensive interactions with WLS (Fig. 1b, c). The complex structure resembles two hands grabbing with each other. WLS looks like a grasping right hand that seizes one finger (hairpin-1) of Wnt3a bearing the

conserved Ser209 site for palmitoleoylation, which is essential for Wnt secretion and interaction with their Frizzled receptors [34]. Wnt3a pinches WLS with another two of its fingers (hairpin -2 and W-loop) at the distal and proximal luminal regions of WLS relative to the membrane, respectively (Fig. 1b, c).

Structural features of WLS

In our model, WLS contains an 8-spanning transmembrane (TM) domain, with both of its N- and C-termini on the cytoplasmic side, and the luminal soluble domain lies between the first and second transmembrane helix (Fig. 2a).

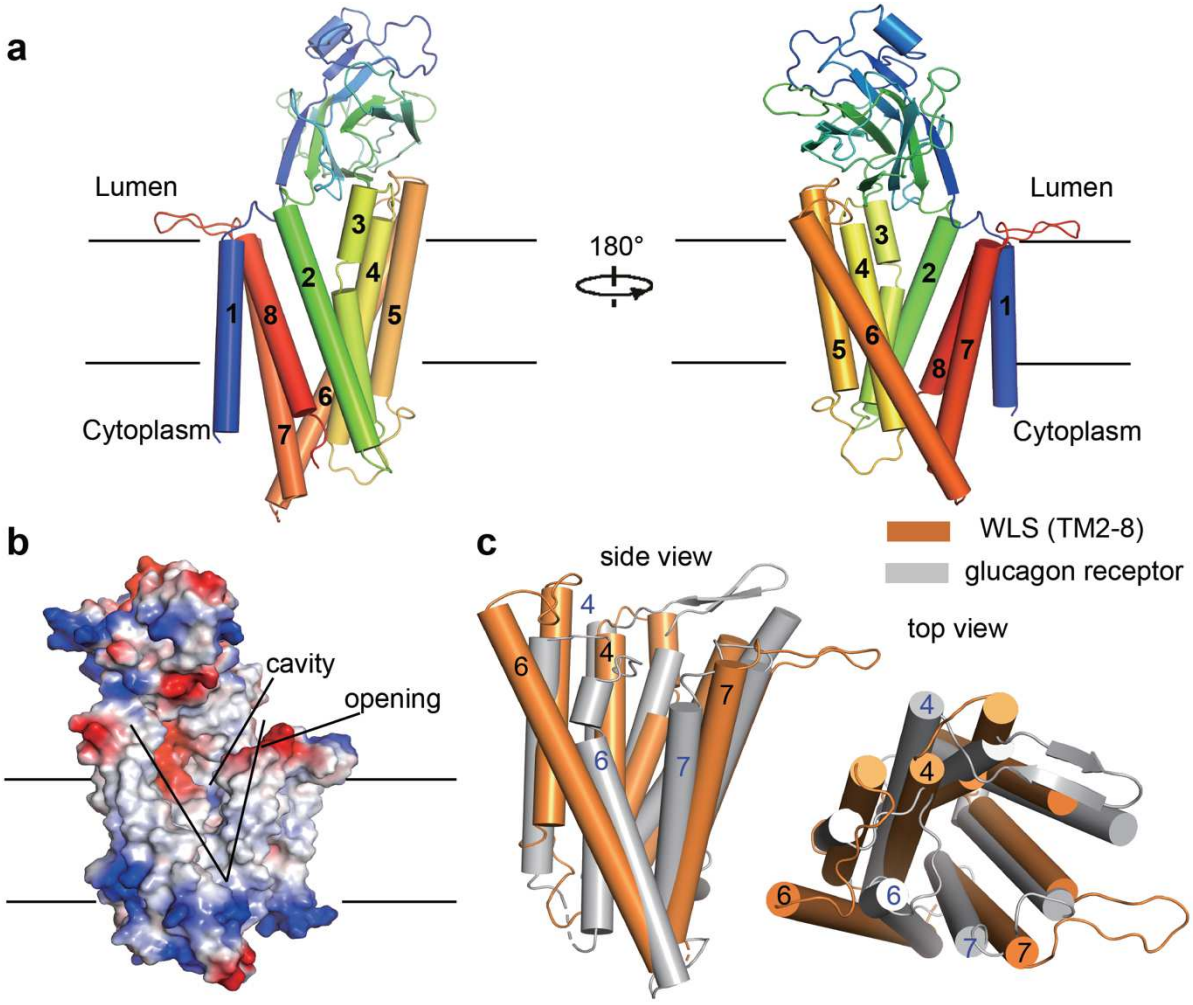

Fig. 2 Structural features of WLS. a Overall structure of WLS. WLS is shown in cartoon with cylindrical helices and rainbow colored. Helix numbers are labeled. **b** Electrostatic analysis result. The cavity and lateral opening are indicated. **c** Superimposition of TM2-8 of WLS and TM region of glucagon receptor. Both side view and top view are shown.

Electrostatic analysis indicates the TM domain of WLS is very hydrophobic, whereas the luminal domain and the cytoplasmic side are highly charged (Fig. 2b). Intriguingly, we found in the TM domain of WLS there is a large hydrophobic cavity and a lateral opening between TM6 and TM7 that exposes the cavity to membrane environment (Fig. 2 a, b). This cavity shields the extruding hairpin-1 of Wnt3a (Fig. 1c).

Using Dali server search, we surprisingly found that TM2-8 of WLS adopt a GPCR fold, though the sequence identity is relatively low (around 10% or even lower). The top results in the ranking list include some well-known representatives of GPCR family, like glucagon receptor[35] (PDB code: 5YQZ), smoothened [36] (PDB code: 6O3C) and Frizzled-4 [37] (PDB code: 6BD4). The superimposition of TM2-8 of WLS and TM region of glucagon receptor mentioned above is shown in the Figure 2c. TM4, TM6 and TM7 in WLS undergo the most dramatic conformational changes compared to glucagon receptor. TM4 moves towards the internal core of WLS, reducing the volume of the internal cavity. TM6 and TM7 separate from each other, generating the lateral opening of WLS.

The luminal domain of WLS (residue range 35 to 229) is arranged into a β-sandwich fold and contains two disulfide bonds that stabilize the structure. The luminal domain shares structural similarity to the monomeric form of a lipid binding protein Seipin[38] (PDB code: 6DS5, Supplementary Fig. 3), which is involved in lipid droplet biogenesis. Although luminal domain of WLS shares structural similarity to a lipid binding protein, no Wnt3a PAM density could be observed in the map of WLS luminal region.

WLS/Wnt3a interaction interfaces

Wnt3a interacts with WLS mainly through three interfaces mediated by hairpin-1 at interface 1, hairpin-2 at interface 2 and W-loop at interface 3, respectively (Fig. 3a). The density in cryo-EM map allowed us to identify some interaction details (Supplementary Fig. 4). At interface 1, diverse interactions are involved: Lys202 of Wnt3a forms electrostatic interaction with Glu178 in luminal domain of WLS (Fig. 3b, left panel); side chain of Lys215 in Wnt3a interact with the main chain of Gln454 in WLS through a hydrogen bond (Fig. 3b, middle

panel); hydrophobic interactions formed by Trp218 of Wnt3a and Ile113, Val222 and Ile224 in the luminal domain of WLS (Fig. 3b, right panel).

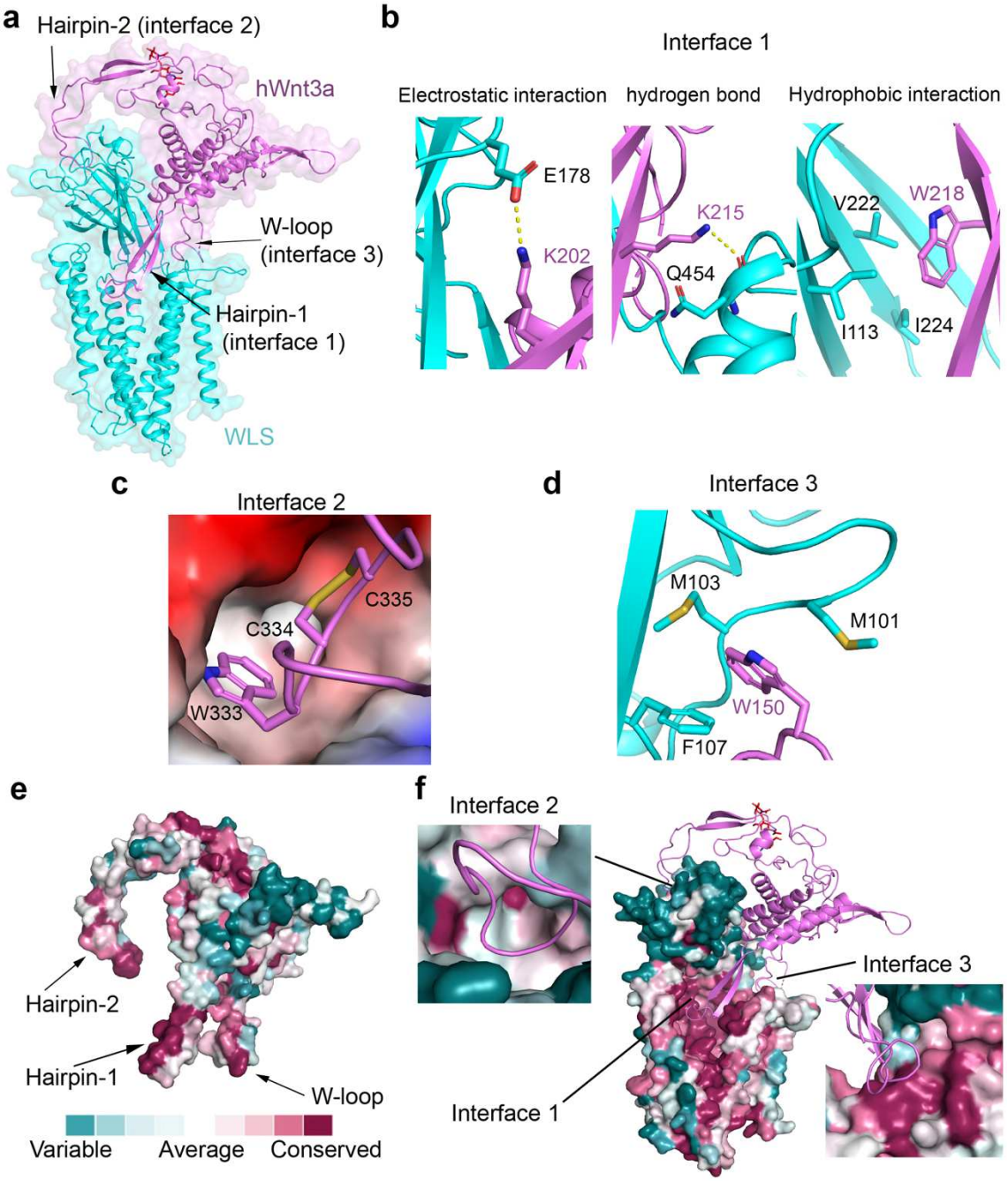

Fig. 3 Interfaces between WLS and Wnt3a. a Three interfaces between WLS and Wnt3a. **b** Interactions at interface 1. From left to right, the three panels represent three types of interactions between WLS and hairpin-1 of Wnt3a: electrostatic interaction, hydrogen bond and hydrophobic interactions, respectively. **c** Interface 2 between hairpin-2 of Wnt3a and a hydrophobic pocket of WLS. **d** Interface 3 between W-loop of Wnt3a and WLS. **e** Conservation surface of Wnt3a. The highly conserved regions involved in binding with WLS are indicated. **f** Conservation surface of WLS. Regions at three interfaces are indicated.

Interface 2 involves hydrophobic interactions between the tip of hairpin-2 containing Trp333 and an adjacent disulfide bond of Wnt3a and a pocket at the distal region of the luminal domain of WLS (Fig. 3c). The tip of Wnt3a hairpin-2 is stabilized by the disulfide bond formed between Cys334 and Cys335. At interface 3, hydrophobic interactions are observed between Trp150 on Wnt3a W-loop and residues of Met101, Met103 and Phe107 in the loop between β-strand 2 (β2) and β-strand 3 (β3) of WLS luminal domain (Fig. 3d).

To further analyze the interactions between Wnt3a and WLS, we generated conservation surface of Wnt3a based on the alignment of all of 19 human Wnt sequences, using the ConSurf server[39] (Fig. 3e and Supplementary Fig. 5). Results show that the three regions of Wnt3a (hairpin-1, hairpin-2, and W-loop) that participate in the interactions with WLS are highly conserved among human Wnts, suggesting all of human Wnts may interact with WLS in a similar manner. We also generated conservation surface for WLS based on the alignment of WLS sequences from various species (Fig. 3f and Supplementary Fig. 6). All of the regions of WLS at the interaction interfaces are conserved. These analysis suggest Wnts probably interact with WLS in a conserved way.

Conformational differences between Wnt3a and Frizzled bound Wnt3

We compared the structures of WLS bound Wnt3a and its close homolog Wnt3 in complex with the cysteine-rich domain of cell surface receptor Frizzled (FZD-CRD) [34,40]. Human Wnt3 (hWnt3, PDB code: 6AHY) clamps FZD-CRD via hairpin-1/W-loop and hairpin-2, and the PAM on Wnt3 directly interact with FZD-CRD (Fig. 4a). Superimposition of structures of Wnt3a and Wnt3 reveals dramatic conformational differences in the loop and hairpin regions of Wnt that are involved in the binding with WLS. Compared to Wnt3a bound with WLS, hairpin-1 of Wnt3 undergoes a 30° rotation, while hairpin-2 and W-loop rotate by about 60° and 90°, respectively (Fig. 4b). This indicates a structural rearrangement of the loop and hairpin regions in Wnt is required during Wnt transfer from WLS to their receptors at cell surface. These structural changes may be a reflection of induced fit when Wnt is bound to different binding partners.

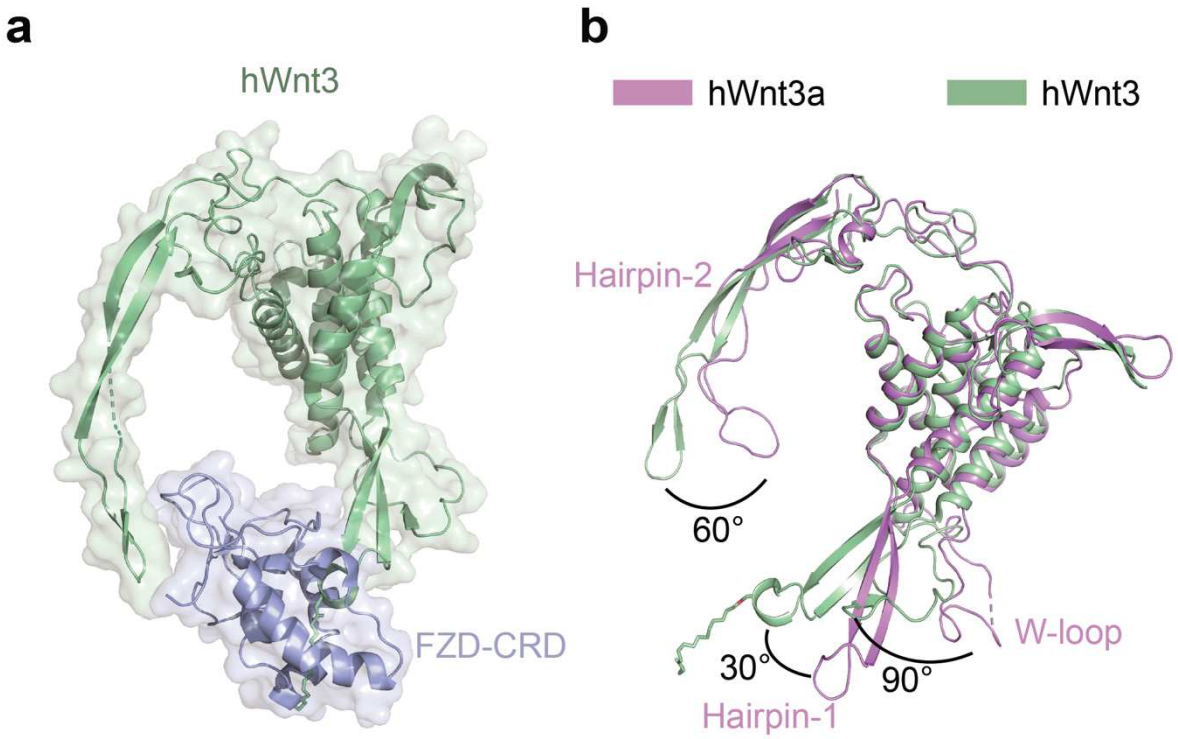

Fig. 4 Comparison between WLS bound Wnt3a and FZD-CRD bound Wnt3. a Structure of hWnt3 in complex with FZD-CRD[40]. **c** Superimposition of hWnt3a and hWnt3.

PAM is not essential for Wnt3a-WLS association

Hairpin-1 of Wnt3a carries the important palmitoleoylation site of Ser209, however, we could only observe extra density possible for PAM that is discontinuous from the density of Ser209 in the cryo-EM map. The possible PAM density lies between TM4 and TM5 with a similar position compared to that in the cryo-EM map of the just released WLS-Wnt8a structure[41] (Supplementary Fig. 7a). There are no obvious conformational changes between WLS in our structure and that in WLS-Wnt8a structure (Supplementary Fig. 7b). We found an empty hydrophobic tunnel between TM4 and TM5 when no molecule was built for the extra density in our map which is in consistence with the structural findings in WLS-Wnt8a structure (Supplementary Fig. 7c). In order to confirm the existence of PAM on Wnt3a in our cryo-EM sample, we detected palmitoleoylation at Ser209 for Wnt3a in our cryo-EM sample by using LC-MS/MS. The double-charged tryptic peptide containing palmitoleoylated Ser209 was detected at 735.381 m/z (highlighted by star) (Fig. 5a). The sequence and modification site in above tryptic peptide was further confirmed by MS/MS analysis (Supplementary Fig. 8). These results suggest that there might be a PAM modified on Ser209 of Wnt3a in our structure.

Wnt3a has extensive interactions with WLS, which we believe should be strong enough to stabilize the binding between these two proteins, though PAM modification on Ser209 may generate more contacts between Wnt3a and WLS. We used co-immunoprecipitation (IP) to examine whether PAM modification on Wnt3a is essential for its association with WLS as it has been reported previously[22,42]. Results showed Wnt3a S209A can be co-immunoprecipitated with WLS, with a slightly lower level compared to WT Wnt3a, whereas no band appeared at the same position of Wnt3a when WLS was co-transfected with a negative control plasmid (Fig. 5b). These results suggest palmitoleoylation on Ser209 is not a prerequisite for the interaction between Wnt3a and WLS, however binding might be weaker due to lack of PAM. Our findings suggest that a lack of PAM on Wnt3a does not disrupt its interaction with WLS. As Wnts are highly conserved (Supplementary Fig. 5), this may also be true for other Wnts.

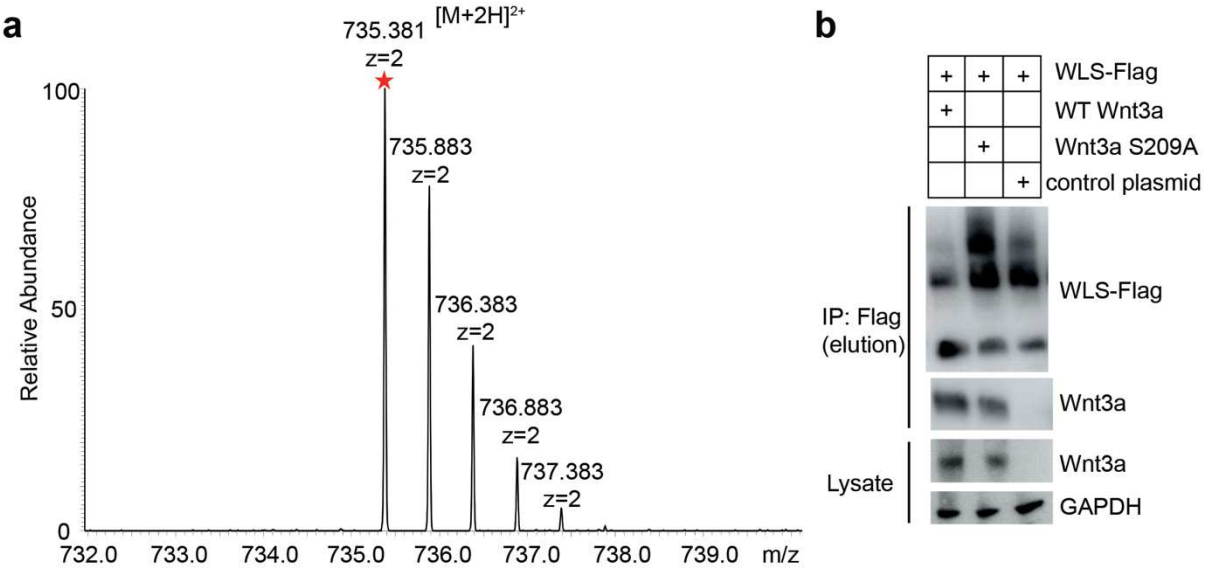

Fig. 5 Palmitoleoylation analysis by mass spectrometry and co-immunoprecipitation analysis. a MS spectra of Wnt3a in cryo-EM sample at the m/z range from 732 to 739. The peak for tryptic peptide containing the PAM modified serine (sequence: CHGLSGSCEVK) is indicated with a star. **b** Co-IP results between WLS and WT Wnt3a or Wnt3a S209A mutant. WLS was C-Flag tagged, and Wnt3a variants were C-terminal His-tagged.

Discussion

We have determined the cryo-EM structure of human WLS-Wnt3a complex. In this structure, TM2-8 of WLS has a GPCR-like fold (Fig. 2c), whereas TM1 may play a structural role and help stabilize the GPCR-like fold and the luminal domain between TM1 and TM2.

Notably, we identified a lateral opening and a large conserved cavity in the TM domain of WLS (Fig. 2b). It is possible that hairpin-1 of Wnt3a enter through this opening to the core cavity, especially when modified with a PAM.

Previous research suggested Wnt hairpin-2 at interface 2 is not essential for WLS mediated Wnt secretion[41,43,44], and we found interface 3 mainly involves limited hydrophobic interactions. Interface 2 and 3 may cooperate with each other to stabilize the interactions at interface 1, and help in later Wnts release and transfer to their receptors. The existence of multiple interacting elements which are structurally switchable (Fig. 4), may serve as a structural base for sequential transfer of these Wnt elements from WLS to FZD-CRD.

One intriguing finding from our study is that lack of PAM on Wnt3a does not disrupt Wnt3a-WLS binding. Previous studies indicated that palmitoleoylation of Wnt on the conserved serine is required for the association between Wnt and WLS [22,42], however our results show that palmitoleoylation on Wnt3a is not essential for the Wnt3a-WLS association, which might be universal for conserved Wnts. Three main interfaces we observed may provide sufficient interactions to form the WLS-Wnt3a complex. Our results suggest the possibility of the existence of a physiological intermediate state during Wnt secretion, in which Wnts may first bind to WLS before the palmitoleoylation occur. In this case, Wnts either need to be released from WLS or more likely undergo conformational changes in the WLS-Wnt complex for hairpin-1 to be palmitoleoylated by Porcupine (Supplementary Fig. 9). Previous research findings suggesting endogenous Porcupine interacts with WLS somewhat support our hypothesis[45].

The structure of WLS-Wnt3a complex we present here provides important insights into understanding of Wnt secretion and signaling. The regions of Wnt3a that are involved in the binding between WLS are highly conserved among all human Wnts, and interfaces on WLS are also conserved among species. These suggest WLS mediated Wnt secretion probably share conserved mechanisms. The luminal domain of WLS provides multiple binding sites for Wnt3a, while the TM domain provides a core cavity which is ideal for accommodation of the tip of hairpin-1 with or without PAM. Our co-IP results showed Wnt3a without PAM can associate with WLS, indicating a possible palmitoleoylation mechanism that may happen on

WLS-bound Wnts. Containing a GPCR fold and the existence of a conserved central cavity make WLS a potential drug target for the treatment of Wnt-driven cancers. Secretion of Wnts also involves some other important regulatory proteins[45,46], for example those participating in vesicle trafficking. How Wnt-WLS complex interact with other regulators, and how Wnts are released from WLS and transferred to their receptors or other extracellular binding proteins remain unclear. More future studies are in need to answer these questions.

Methods

Protein expression and purification

cDNA of human WLS, Wnt3a and Porcupine were cloned into PEG BacMam vector[29] (gifted from Dr. Eric Gouaux) and bearing C-terminal Flag tag, 10xhis tag and GFP-Flag tag, respectively. BacMam viruses were generated through standard methods and batches of P4 were used for transfection of HEK293S GnTI$^-$ cells. Plasmid containing Porcupine was transiently transfected into HEK293S GnTI$^-$ cells at density of 2.0×10^6/ml. Then volume ratio of 1: 4 for viruses of WLS and Wnt3a were supplemented. After 8-12 hours of post-transfection, 10 mM of sodium butyrate and 100 nM of bafilomycin A1 was supplemented and culture temperature was lowered to 30 °C. After another 48 hours, cells were harvested and resuspended with lysis buffer containing 25 mM Tris, pH 8.0, 150 mM NaCl and protease inhibitors including Aprotinin, Pepstatin, Leupeptin and PMSF. Cells were disrupted by sonication followed by adding detergent GDN at final concentration (w/v) of 1% for membrane protein extraction at 4 °C for 2 hours. After centrifugation at 100,000 g for 1 hour, we collected the supernatant for further purification by anti-Flag agarose and then nickel resin before run gel filtration in buffer containing 25 mM Tris, pH 8.0 and 150 mM NaCl and 0.03% GDN.

Cryo-EM sample preparation and data collection

The purified WLS-Wnt3a complex at concentration of 0.19 mg/ml was used for cryo-EM sample preparation. Holey carbon grids (Quantifoil Au R1.2/1.3) were coated with a thin layer of graphene oxide. Grids were glow-discharged before applying of 3 μl of protein sample followed by a 5 sec blotting using Vitrobot (Mark IV, ThermoFisher Scientific). After blotting, grids were rapidly immersed into pre-cooled liquid ethane and transferred to liquid nitrogen.

Data acquisition was done on Titan Krios operating at 300 kV equipped with Gatan K3 Summit detector and GIF Quantum energy filter at 81,000× magnification. Movie stacks were automatically acquired with a 20 eV slit width and a defocus range from −1.5 to −1.8 μm. Each stack consisting of 32 frames was exposed for 2.56 sec with total dose of ~50 $e^{-}/Å^2$.

Data processing

A total of 6,757,877 particles were automatically picked by RELION 3.0[47-49] from 12,578 micrographs. Three rounds of 2D classification gave rise to an initial model with 683,203 particles. We then carried out several rounds of 3D classification, including the "guided multi-reference classification", which used the best reference and some bad ones that were phase-randomized or region-fragmented. The steps above resulted in a map with more distinct features. The strong noise from micelle impeded the further progressing of the resolution. To overcome this boundedness, we created a mask that encompassed both the micelle and protein, but the region of micelle was weighted to 0.8 or 0.6. Focused refinement using this mask leaded to a breakthrough of resolution to 5.2 Å. We then used this map to rescue good particles back using another two rounds of 3D classification. After re-extracting particles without binning, a new 3D refinement brought the resolution up to 4.3 Å.

Finally, detailed inspection of the density in the map suggested that there were several high value spots which broke the balance in 3D reconstruction. As a consequence, we manually "corrected" the map by reducing the extreme value on those spots. A data set of 141,917 particles contributed to a final map of 3.8 Å (supplementary Fig. 1, 2). The resolution was estimated with the gold-standard Fourier shell correlation 0.143 criterion[50] with high-resolution noise substitution[51].

Model building and refinement

The atomic coordinate of the WLS/Wnt3a complex was generated by combining homology modeling and de novo model building. An initial structure model of WLS TM2-8 and luminal domain was firstly predicted by trRosetta[31] and tFold[32]. TM1 of WLS was generated using SWISS-MODEL online server[52]. The template used for the homology modeling of Wnt3a was hWnt3 from Wnt-frizzled (CRD) complex[40] (PDB code: 6AHY). The models were firstly

docked into the final reconstruction map in Chimera[53] and then manually adjusted in COOT[54]. Subsequently, the models were refined and relaxed into density maps using Rosetta[55,56].

The improved model of WLS/Wnt3a complex was refined against the corresponding map using PHENIX[57] in real space with secondary structure and geometry restraints. Overfitting of model was monitored by refining the model in one of the two independent maps from the gold-standard refinement approach, and testing the refined model against the other map[58]. The structure of WLS/Wnt3a complex was validated through examination of the Molprobity scores and statistics of the Ramachandran plots (Supplementary Table 1). Molprobity scores were calculated as described[59].

Mass spectrometry analysis

The SDS-PAGE was used to separate the protein, and stained with Coomassie Blue G-250. The gel bands of interest were cut into pieces. Sample was digested by trypsin with prior reduction and alkylation in 50 mM ammonium bicarbonate at 37ºC overnight. The digested products were extracted twice with 1% formic acid in 50% acetonitrile aqueous solution and dried to reduce volume by speedvac.

For LC-MS/MS analysis, the peptides were separated by a 65 min gradient elution at a flow rate 0.300 µL/min with the Thermo EASY-nLC1200 integrated nano-HPLC system which is directly interfaced with the Thermo Q Exactive HF-X mass spectrometer. The analytical column was a home-made fused silica capillary column (75 µm ID, 150 mm length; Upchurch, Oak Harbor, WA) packed with C-18 resin (300 A, 3 µm, Varian, Lexington, MA). Mobile phase A consisted of 0.1% formic acid, and mobile phase B consisted of 100% acetonitrile and 0.1% formic acid. The mass spectrometer was operated in the data-dependent acquisition mode using the Xcalibur 4.1 software and there is a single full-scan mass spectrum in the Orbitrap (400-1800 m/z, 60,000 resolution) followed by 20 data-dependent MS/MS scans at 30% normalized collision energy. Each mass spectrum was analyzed using the Thermo Xcalibur Qual Browser and Proteome Discovery for the database searching.

Co-immunoprecipitation

cDNA of WT Wnt3a and Wnt3a S209A bearing C-terminal 10xhis tag, and WT WLS bearing C-Flag tag were constructed into vectors for transient transfection of Hela cells. Cells were plated in six-well dishes, and cells in each well were transfected with 2.5 ug plasmids containing Wnt3a (either WT or S209A mutant) and WT WLS at w/w ratio of 4:1 using lipofectamine 3000 as the transfection reagent. After 36 hours of post-transfection, cells were washed with PBS buffer and resuspended with buffer containing 25 mM Tris pH 8.0, 150 mM NaCl and 1% Triton X-100, and protease inhibitors of Aprotinin, Pepstatin, Leupeptin and PMSF. The cell suspension was incubated at 4 °C for 1 hour to disrupt cells and extract total membrane proteins, following by centrifugation at 100,000 g to remove cell debris. Supernatant was loaded to anti-Flag agarose twice and the resin was washed with 4X10 volumes of buffer containing 25 mM Tris pH 8.0, 300 mM NaCl, 0.1% Triton X-100. We used wash buffer supplemented with 0.4 mg/ml of Flag peptide to elute proteins from the resin. Cell lysate and elution samples were used for western blotting analysis.

Acknowledgements

We would like to thank the Cryo-EM Facility of Westlake University for providing cryo-EM and computation support. We thank Westlake University Supercomputer Center for computational resources and related assistance. We thank the Mass Spectrometry & Metabolomics Core Facility of the Center for Biomedical Research Core Facilities of Westlake University for sample analysis. We thank Dr. Eric Gouaux (Oregon Health & Science University) for kindly sharing the plasmid of pEG BacMam. We thank Dr. Jianping Wu for discussion during model building. We thank Dr. Hongtao Yu and Dr. Dangsheng Li for suggestions on manuscript preparation. This work was supported by Westlake Education Foundation. This work was also supported by National Natural Science Foundation of China (Project No. 31900113).

Author Contributions

D.M. conceived the project. D.M. and Q.Z. (Qiang Zhou) designed experiments and supervised the project. Q.Z. (Qing Zhong) did protein expression and purification, cryo-EM

sample preparation, data collection, and functional assays. F.Y. performed cryo-EM data processing. Z.X. did model building and refinement. Y.Z. and G.H. helped in data processing. X.Z. (Xiechao Zhan) helped in model building. K.S. predicted initial model with Rosetta and did model relax. Z.W. and S.C. set up assay system and did initial test. S.F. and X.Z (Xiuxiu Zhao) performed mass spectrometry analysis. J.Z. predicted initial model with tFold. M.X. helped in functional assays. P.L. and W.X. contributed to data analysis and discussion. D.M. wrote the manuscript.

Competing financial interests

The authors declare no competing financial interests.

Reference

1 Loh, K. M., van Amerongen, R. & Nusse, R. Generating Cellular Diversity and Spatial Form: Wnt Signaling and the Evolution of Multicellular Animals. *Dev Cell* **38**, 643-655, doi:10.1016/j.devcel.2016.08.011 (2016).

2 Komiya, Y. & Habas, R. Wnt signal transduction pathways. *Organogenesis* **4**, 68-75, doi:10.4161/org.4.2.5851 (2008).

3 Clevers, H. Wnt/beta-catenin signaling in development and disease. *Cell* **127**, 469-480, doi:10.1016/j.cell.2006.10.018 (2006).

4 Steinhart, Z. & Angers, S. Wnt signaling in development and tissue homeostasis. *Development* **145**, doi:10.1242/dev.146589 (2018).

5 Clevers, H. & Nusse, R. Wnt/β-catenin signaling and disease. *Cell* **149**, 1192-1205, doi:10.1016/j.cell.2012.05.012 (2012).

6 Zhan, T., Rindtorff, N. & Boutros, M. Wnt signaling in cancer. *Oncogene* **36**, 1461-1473, doi:10.1038/onc.2016.304 (2017).

7 Mikels, A. J. & Nusse, R. Wnts as ligands: processing, secretion and reception. *Oncogene* **25**, 7461-7468, doi:10.1038/sj.onc.1210053 (2006).

8 Willert, K. & Nusse, R. Wnt proteins. *Cold Spring Harb Perspect Biol* **4**, a007864, doi:10.1101/cshperspect.a007864 (2012).

9 MacDonald, B. T., Tamai, K. & He, X. Wnt/beta-catenin signaling: components, mechanisms, and diseases. *Dev Cell* **17**, 9-26, doi:10.1016/j.devcel.2009.06.016 (2009).

10 MacDonald, B. T. & He, X. Frizzled and LRP5/6 receptors for Wnt/β-catenin signaling. *Cold Spring Harb Perspect Biol* **4**, doi:10.1101/cshperspect.a007880 (2012).

11 Niehrs, C. The complex world of WNT receptor signalling. *Nat Rev Mol Cell Biol* **13**, 767-779, doi:10.1038/nrm3470 (2012).

12 van Amerongen, R., Mikels, A. & Nusse, R. Alternative wnt signaling is initiated by distinct receptors. *Sci Signal* **1**, re9, doi:10.1126/scisignal.135re9 (2008).

13 Parchure, A., Vyas, N. & Mayor, S. Wnt and Hedgehog: Secretion of Lipid-Modified Morphogens. *Trends Cell Biol* **28**, 157-170, doi:10.1016/j.tcb.2017.10.003 (2018).

14 Takada, R. *et al.* Monounsaturated fatty acid modification of Wnt protein: its role in Wnt secretion. *Dev Cell* **11**, 791-801, doi:10.1016/j.devcel.2006.10.003 (2006).
15 Hofmann, K. A superfamily of membrane-bound O-acyltransferases with implications for wnt signaling. *Trends Biochem Sci* **25**, 111-112, doi:10.1016/s0968-0004(99)01539-x (2000).
16 Willert, K. *et al.* Wnt proteins are lipid-modified and can act as stem cell growth factors. *Nature* **423**, 448-452, doi:10.1038/nature01611 (2003).
17 Zhai, L., Chaturvedi, D. & Cumberledge, S. Drosophila wnt-1 undergoes a hydrophobic modification and is targeted to lipid rafts, a process that requires porcupine. *J Biol Chem* **279**, 33220-33227, doi:10.1074/jbc.M403407200 (2004).
18 Bänziger, C. *et al.* Wntless, a conserved membrane protein dedicated to the secretion of Wnt proteins from signaling cells. *Cell* **125**, 509-522, doi:10.1016/j.cell.2006.02.049 (2006).
19 Bartscherer, K., Pelte, N., Ingelfinger, D. & Boutros, M. Secretion of Wnt ligands requires Evi, a conserved transmembrane protein. *Cell* **125**, 523-533, doi:10.1016/j.cell.2006.04.009 (2006).
20 Goodman, R. M. *et al.* Sprinter: a novel transmembrane protein required for Wg secretion and signaling. *Development* **133**, 4901-4911, doi:10.1242/dev.02674 (2006).
21 Fu, J., Jiang, M., Mirando, A. J., Yu, H. M. & Hsu, W. Reciprocal regulation of Wnt and Gpr177/mouse Wntless is required for embryonic axis formation. *Proc Natl Acad Sci U S A* **106**, 18598-18603, doi:10.1073/pnas.0904894106 (2009).
22 Coombs, G. S. *et al.* WLS-dependent secretion of WNT3A requires Ser209 acylation and vacuolar acidification. *J Cell Sci* **123**, 3357-3367, doi:10.1242/jcs.072132 (2010).
23 Belenkaya, T. Y. *et al.* The retromer complex influences Wnt secretion by recycling wntless from endosomes to the trans-Golgi network. *Dev Cell* **14**, 120-131, doi:10.1016/j.devcel.2007.12.003 (2008).
24 Franch-Marro, X. *et al.* Wingless secretion requires endosome-to-Golgi retrieval of Wntless/Evi/Sprinter by the retromer complex. *Nat Cell Biol* **10**, 170-177, doi:10.1038/ncb1678 (2008).
25 Port, F. *et al.* Wingless secretion promotes and requires retromer-dependent cycling of Wntless. *Nat Cell Biol* **10**, 178-185, doi:10.1038/ncb1687 (2008).
26 Stewart, J. *et al.* Analysis of wntless (WLS) expression in gastric, ovarian, and breast cancers reveals a strong association with HER2 overexpression. *Mod Pathol* **28**, 428-436, doi:10.1038/modpathol.2014.114 (2015).
27 Seo, J. *et al.* Inhibition of Wntless/GPR177 suppresses gastric tumorigenesis. *BMB Rep* **51**, 255-260, doi:10.5483/bmbrep.2018.51.5.046 (2018).
28 Anastas, J. N. & Moon, R. T. WNT signalling pathways as therapeutic targets in cancer. *Nat Rev Cancer* **13**, 11-26, doi:10.1038/nrc3419 (2013).
29 Goehring, A. *et al.* Screening and large-scale expression of membrane proteins in mammalian cells for structural studies. *Nat Protoc* **9**, 2574-2585, doi:10.1038/nprot.2014.173 (2014).
30 George, A., Leahy, H., Zhou, J. & Morin, P. J. The vacuolar-ATPase inhibitor bafilomycin and mutant VPS35 inhibit canonical Wnt signaling. *Neurobiol Dis* **26**, 125-133, doi:10.1016/j.nbd.2006.12.004 (2007).
31 Yang, J. *et al.* Improved protein structure prediction using predicted interresidue orientations. *Proc Natl Acad Sci U S A* **117**, 1496-1503, doi:10.1073/pnas.1914677117 (2020).
32 Xiao, Q. *et al.* Structure of human steroid 5α-reductase 2 with anti-androgen drug finasteride. *Res Sq*, doi:10.21203/rs.3.rs-40159/v1 (2020).

33 DeLano, W. L. *The PyMOL Molecular Graphics System.*, <http://www.pymol.org> (2002).
34 Janda, C. Y., Waghray, D., Levin, A. M., Thomas, C. & Garcia, K. C. Structural basis of Wnt recognition by Frizzled. *Science* **337**, 59-64, doi:10.1126/science.1222879 (2012).
35 Zhang, H. *et al.* Structure of the glucagon receptor in complex with a glucagon analogue. *Nature* **553**, 106-110, doi:10.1038/nature25153 (2018).
36 Deshpande, I. *et al.* Smoothened stimulation by membrane sterols drives Hedgehog pathway activity. *Nature* **571**, 284-288, doi:10.1038/s41586-019-1355-4 (2019).
37 Yang, S. *et al.* Crystal structure of the Frizzled 4 receptor in a ligand-free state. *Nature* **560**, 666-670, doi:10.1038/s41586-018-0447-x (2018).
38 Yan, R. *et al.* Human SEIPIN Binds Anionic Phospholipids. *Dev Cell* **47**, 248-256.e244, doi:10.1016/j.devcel.2018.09.010 (2018).
39 Glaser, F. *et al.* ConSurf: identification of functional regions in proteins by surface-mapping of phylogenetic information. *Bioinformatics* **19**, 163-164, doi:10.1093/bioinformatics/19.1.163 (2003).
40 Hirai, H., Matoba, K., Mihara, E., Arimori, T. & Takagi, J. Crystal structure of a mammalian Wnt-frizzled complex. *Nat Struct Mol Biol* **26**, 372-379, doi:10.1038/s41594-019-0216-z (2019).
41 Nygaard, R. *et al.* Structural Basis of WLS/Evi-Mediated Wnt Transport and Secretion. *Cell*, doi:10.1016/j.cell.2020.11.038 (2020).
42 Herr, P. & Basler, K. Porcupine-mediated lipidation is required for Wnt recognition by Wls. *Dev Biol* **361**, 392-402, doi:10.1016/j.ydbio.2011.11.003 (2012).
43 Wu, C. H. & Nusse, R. Ligand receptor interactions in the Wnt signaling pathway in Drosophila. *J Biol Chem* **277**, 41762-41769, doi:10.1074/jbc.M207850200 (2002).
44 Kumar, S. *et al.* Molecular dissection of Wnt3a-Frizzled8 interaction reveals essential and modulatory determinants of Wnt signaling activity. *BMC Biol* **12**, 44, doi:10.1186/1741-7007-12-44 (2014).
45 Glaeser, K. *et al.* ERAD-dependent control of the Wnt secretory factor Evi. *Embo j* **37**, doi:10.15252/embj.201797311 (2018).
46 Sun, J. *et al.* A Wntless-SEC12 complex on the ER membrane regulates early Wnt secretory vesicle assembly and mature ligand export. *J Cell Sci* **130**, 2159-2171, doi:10.1242/jcs.200634 (2017).
47 Zivanov, J. *et al.* New tools for automated high-resolution cryo-EM structure determination in RELION-3. *Elife* **7**, doi:10.7554/eLife.42166 (2018).
48 Kimanius, D., Forsberg, B. O., Scheres, S. H. & Lindahl, E. Accelerated cryo-EM structure determination with parallelisation using GPUs in RELION-2. *Elife* **5**, doi:10.7554/eLife.18722 (2016).
49 Scheres, S. H. RELION: implementation of a Bayesian approach to cryo-EM structure determination. *J Struct Biol* **180**, 519-530, doi:10.1016/j.jsb.2012.09.006 (2012).
50 Rosenthal, P. B. & Henderson, R. Optimal determination of particle orientation, absolute hand, and contrast loss in single-particle electron cryomicroscopy. *J Mol Biol* **333**, 721-745, doi:10.1016/j.jmb.2003.07.013 (2003).
51 Chen, S. *et al.* High-resolution noise substitution to measure overfitting and validate resolution in 3D structure determination by single particle electron cryomicroscopy. *Ultramicroscopy* **135**, 24-35, doi:10.1016/j.ultramic.2013.06.004 (2013).

52 Waterhouse, A. *et al.* SWISS-MODEL: homology modelling of protein structures and complexes. *Nucleic Acids Res* **46**, W296-w303, doi:10.1093/nar/gky427 (2018).
53 Pettersen, E. F. *et al.* UCSF Chimera--a visualization system for exploratory research and analysis. *J Comput Chem* **25**, 1605-1612, doi:10.1002/jcc.20084 (2004).
54 Emsley, P. & Cowtan, K. Coot: model-building tools for molecular graphics. *Acta Crystallogr D Biol Crystallogr* **60**, 2126-2132, doi:10.1107/s0907444904019158 (2004).
55 Frenz, B., Walls, A. C., Egelman, E. H., Veesler, D. & DiMaio, F. RosettaES: a sampling strategy enabling automated interpretation of difficult cryo-EM maps. *Nat Methods* **14**, 797-800, doi:10.1038/nmeth.4340 (2017).
56 Wang, R. Y. *et al.* Automated structure refinement of macromolecular assemblies from cryo-EM maps using Rosetta. *Elife* **5**, doi:10.7554/eLife.17219 (2016).
57 Afonine, P. V. *et al.* Real-space refinement in PHENIX for cryo-EM and crystallography. *Acta Crystallogr D Struct Biol* **74**, 531-544, doi:10.1107/s2059798318006551 (2018).
58 Amunts, A. *et al.* Structure of the yeast mitochondrial large ribosomal subunit. *Science* **343**, 1485-1489, doi:10.1126/science.1249410 (2014).
59 Davis, I. W. *et al.* MolProbity: all-atom contacts and structure validation for proteins and nucleic acids. *Nucleic Acids Res* **35**, W375-383, doi:10.1093/nar/gkm216 (2007).

Figures

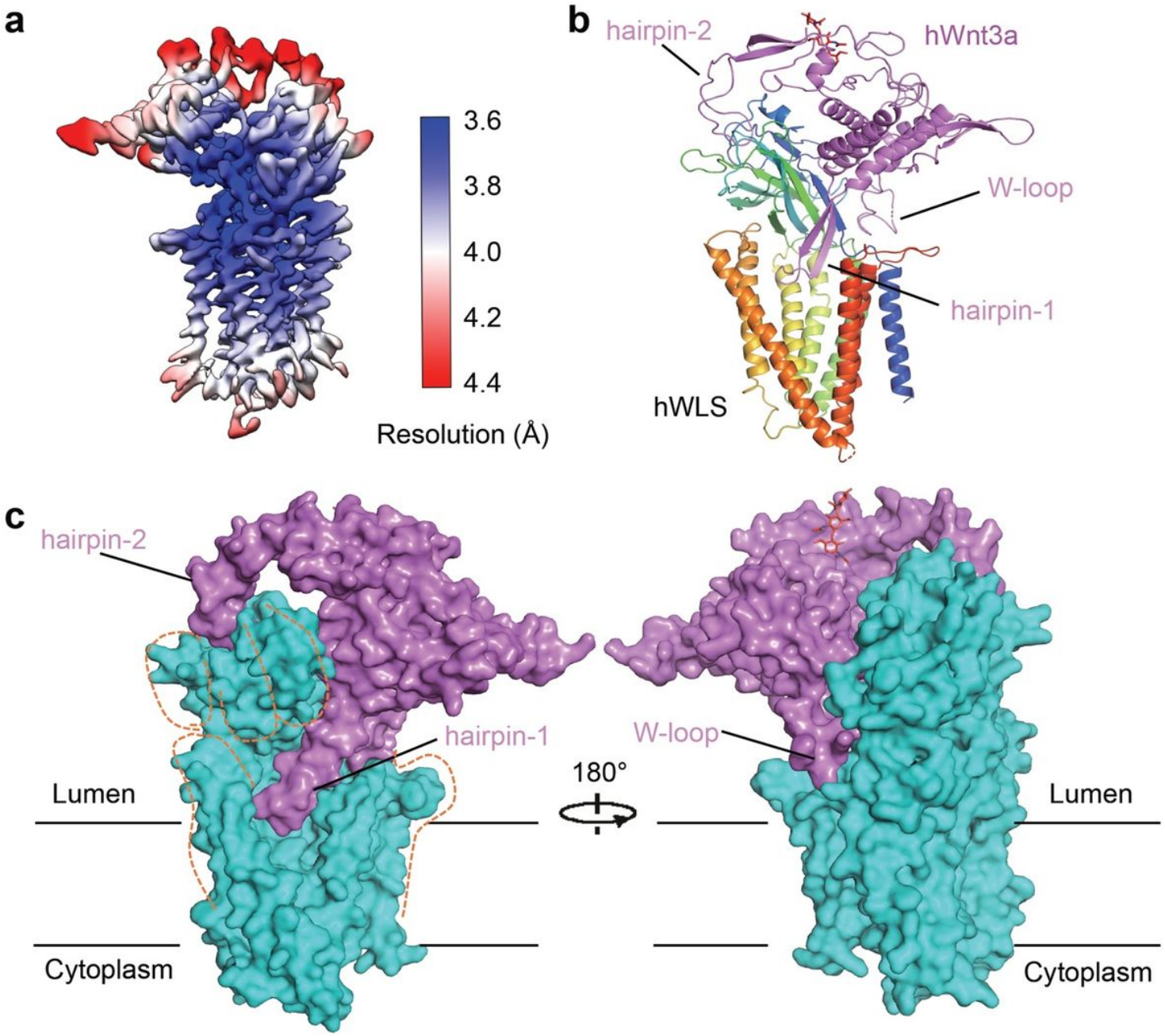

Figure 1

Cryo-EM structure of human WLS in complex with Wnt3a. a Local resolution map of WLS-Wnt3a complex estimated with RELION. b Overall structure of the WLS-Wnt3a complex. WLS is shown in cartoon and colored in rainbow, with N-termini in blue and C-termini in red. Wnt3a is colored in magenta. The sugar moiety on Wnt3a is shown as sticks. c Complex structure is shown in surface with Wnt3a colored in magenta and WLS colored in cyan. The contour of hand shape of WLS is shown in orange dash lines. All structural figures are generated with PyMOL33.

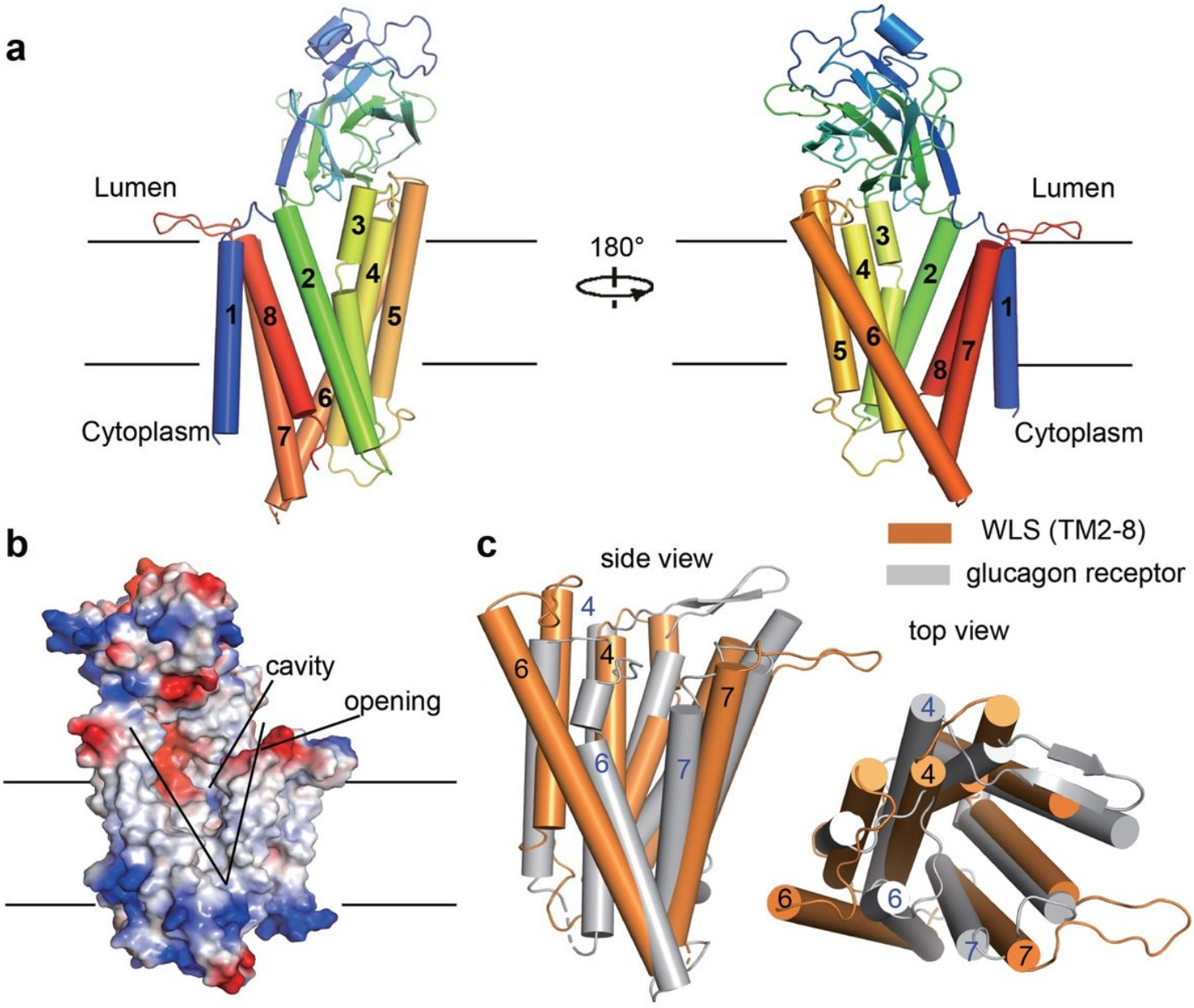

Figure 2

Structural features of WLS. a Overall structure of WLS. WLS is shown in cartoon with cylindrical helices and rainbow colored. Helix numbers are labeled. b Electrostatic analysis result. The cavity and lateral opening are indicated. c Superimposition of TM2-8 of WLS and TM region of glucagon receptor. Both side view and top view are shown.

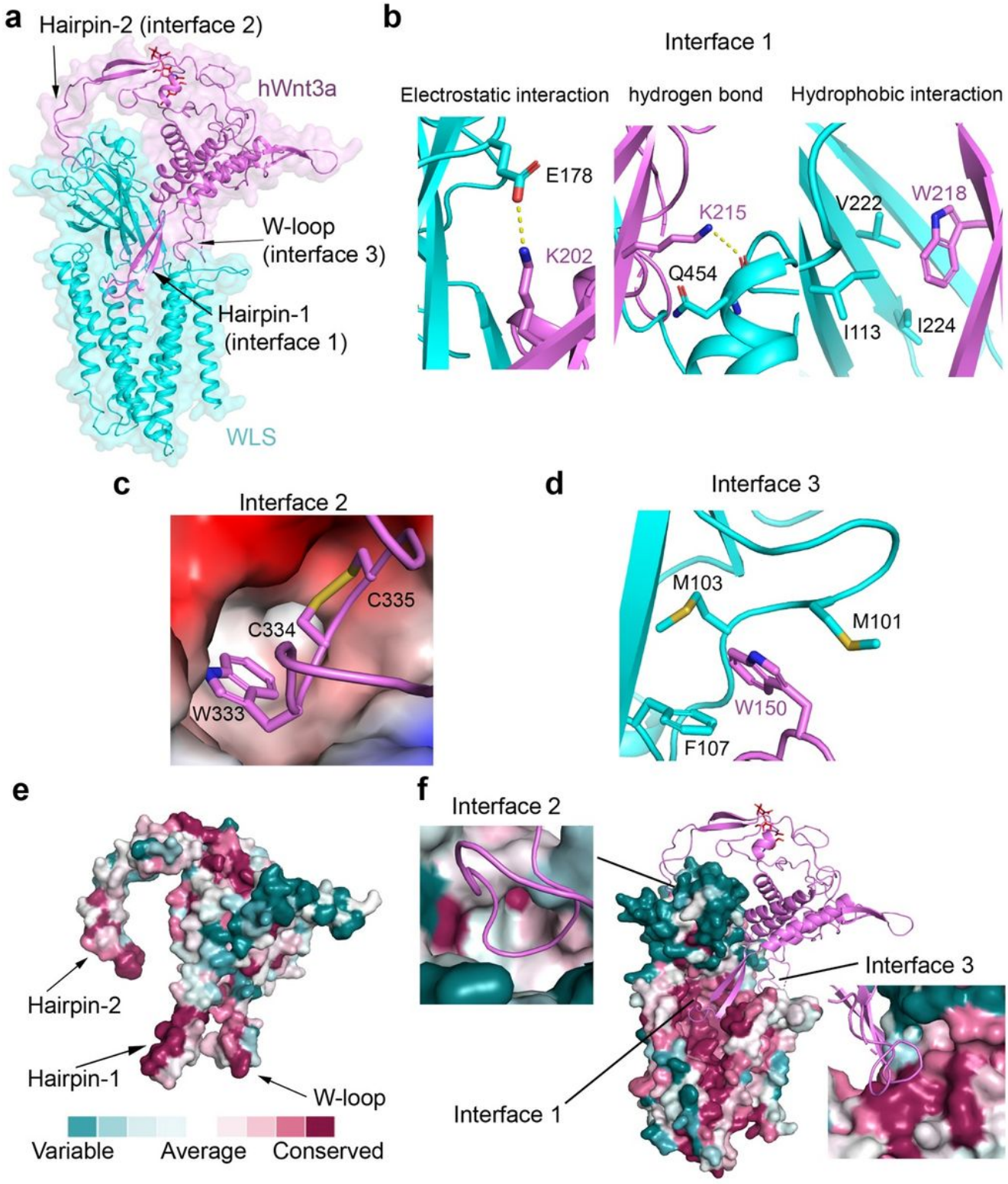

Figure 3

Interfaces between WLS and Wnt3a. a Three interfaces between WLS and Wnt3a. b Interactions at interface 1. From left to right, the three panels represent three types of interactions between WLS and hairpin-1 of Wnt3a: electrostatic interaction, hydrogen bond and hydrophobic interactions, respectively. c Interface 2 between hairpin-2 of Wnt3a and a hydrophobic pocket of WLS. d Interface 3 between W-loop

of Wnt3a and WLS. e Conservation surface of Wnt3a. The highly conserved regions involved in binding with WLS are indicated. f Conservation surface of WLS. Regions at three interfaces are indicated.

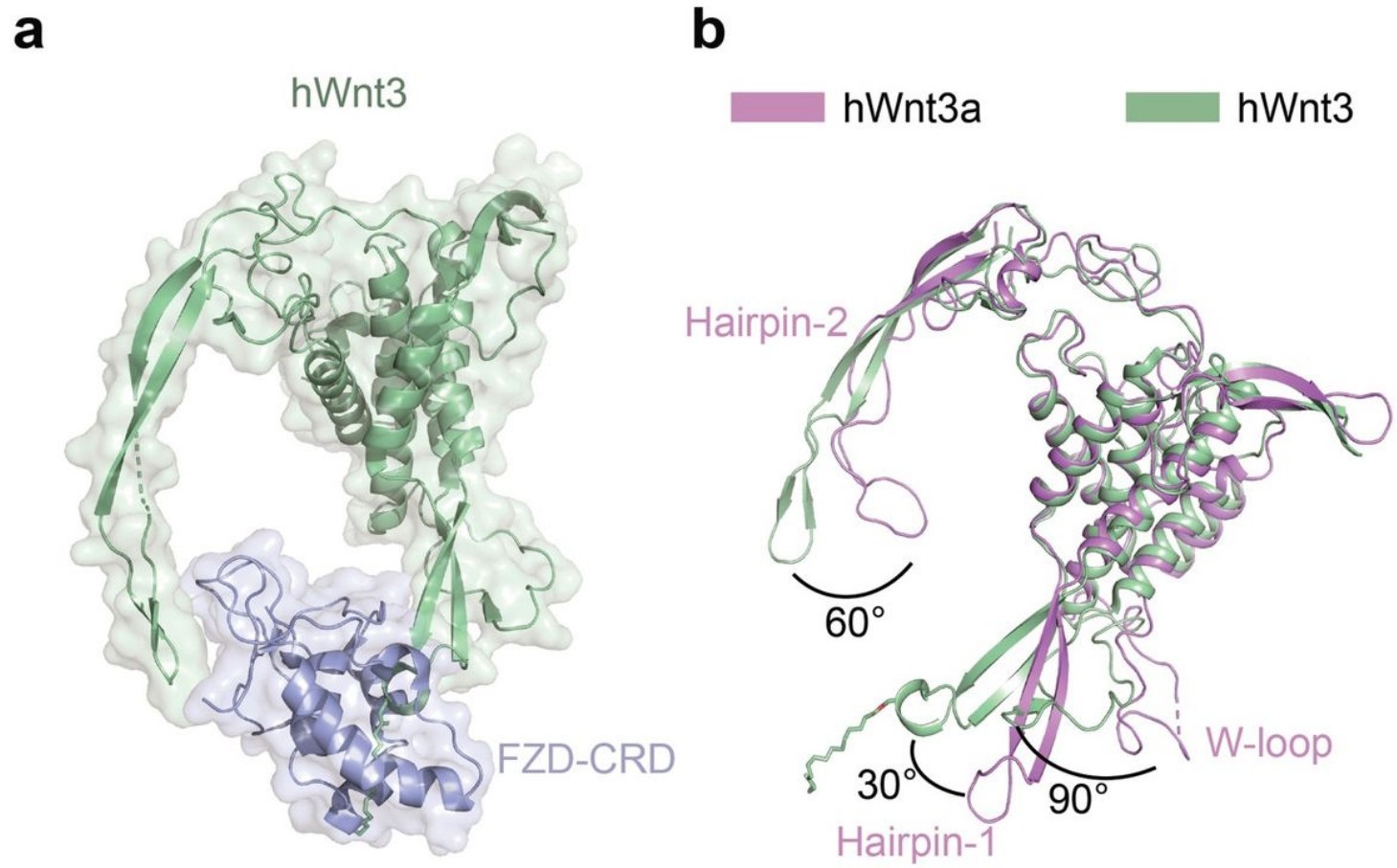

Figure 4

Comparison between WLS bound Wnt3a and FZD-CRD bound Wnt3. a Structure of hWnt3 in complex with FZD-CRD40. c Superimposition of hWnt3a and hWnt3.

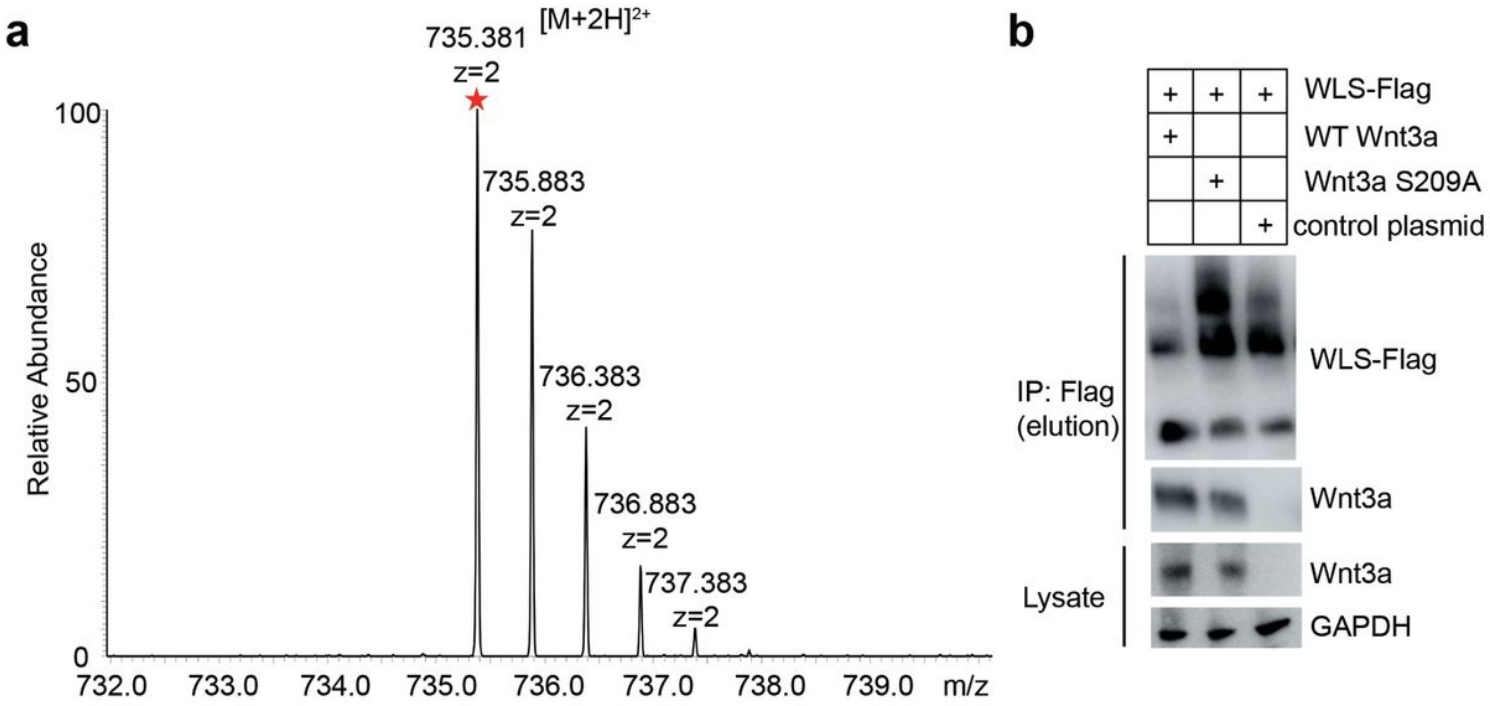

Figure 5

Palmitoleoylation analysis by mass spectrometry and co-immunoprecipitation analysis. a MS spectra of Wnt3a in cryo-EM sample at the m/z range from 732 to 739. The peak for tryptic peptide containing the PAM modified serine (sequence: CHGLSGSCEVK) is indicated with a star. b Co-IP results between WLS and WT Wnt3a or Wnt3a S209A mutant. WLS was C-Flag tagged, and Wnt3a variants were C-terminal His-tagged.

Supplementary Files

This is a list of supplementary files associated with this preprint. Click to download.

- SupplementaryinformationDM.pdf